Research article

Design and preparation of a novel Mg–Al LDH@EDTA-Melamine nanocomposite for effective adsorptive removal of methylene blue and rhodamine B dyes from water

Mohammad Ara , Hossein Ghafuri [*]

Catalysts and Organic Synthesis Research Laboratory, Department of Chemistry, Iran University of Science and Technology, Tehran, 16846-13114, Iran

A B S T R A C T

This paper deals with the preparation of a novel nanocomposite consisted of magnesium-aluminum layered double hydroxide (Mg–Al LDH) and ethylenediaminetetraacetic acid (EDTA) as well as melamine (MA) as an adsorbent. This nanocomposite was utilized to adsorb different dyes such as rhodamine B (RhB) and methylene blue (MB) from water. The prepared adsorbent was characterized using FT-IR, EDS, XRD, TGA, and FE-SEM analyses. The effects of various parameters such as concentration, time, adsorbent dosage, temperature, and pH were tested to investigate their influence on adsorption conditions. Both methylene blue and rhodamine B dyes showed pseudo-second-order adsorption kinetics, and their adsorption followed the Langmuir isotherm. Moreover, the maximum adsorption capacities for methylene blue and rhodamine B were found to be 1111.103 mg/g at 45 °C and 232.558 mg/g at 60 °C, respectively. Additionally, the adsorption processes were found to be spontaneous ($\Delta G° < 0$, for both dyes) and exothermic ($\Delta H° = -12.42$ kJ/mol for methylene blue and $\Delta H° = -25.84$ kJ/mol for rhodamine B) for both dyes. Hydrogen bonding and electrostatic forces are responsible for the interactions occur between the nanocomposite and the functional groups in the dyes. The experimental findings demonstrated a greater adsorption rate of MB than RhB, suggesting the adsorbent's stronger affinity for MB. This preference is likely due to MB's size, specific functional groups, and smaller molecule size, enabling stronger interactions and more efficient access to adsorption sites compared to RhB. Even after recycling 4 times, the dye adsorption percentages of the adsorbent for MB and RhB dyes were 90 % and 87 %, but the desorption percentages of the adsorbate dyes were 85 % and 80 %, respectively. The prepared adsorbent boasts several unique properties, such as the swift and effortless adsorption of MB and RhB dyes, straightforward synthesis, mild adsorption conditions, remarkable efficiency, and the ability to be recycled up to 4 times without a significant decrease in activity.

1. Introduction

Industrialization, while addressing the needs of society and contributing to the development of countries, also brings about challenges, such as environmental pollution [1–3]. Dyes are important chemical compounds that degrade slowly [4,5]. Dyes have

---
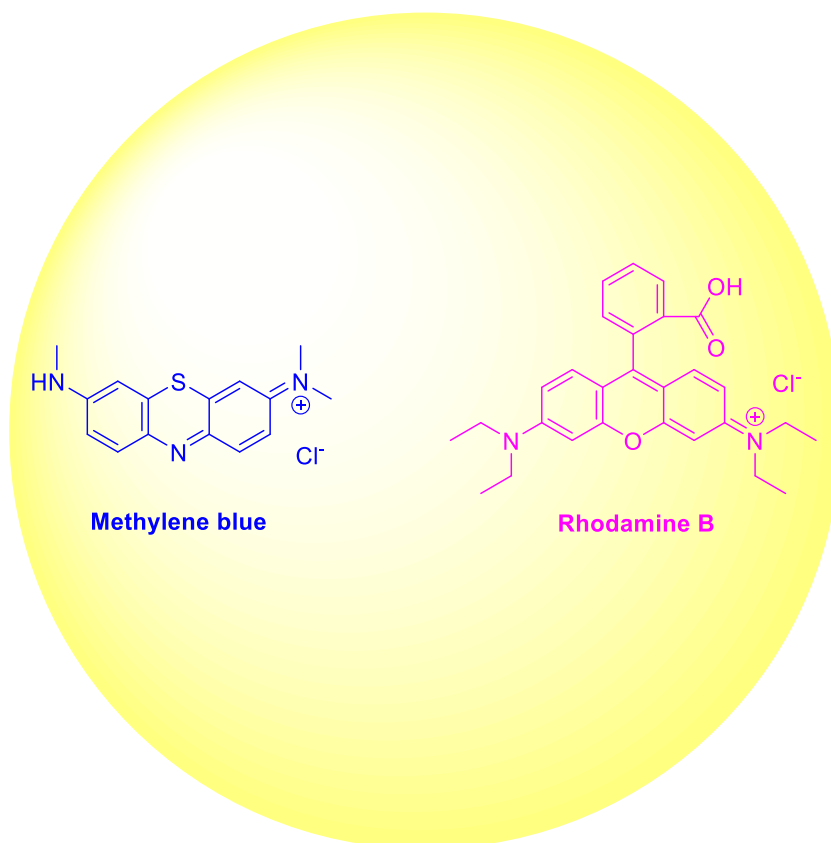
Scheme 1. The chemical structure of methylene blue and rhodamine B dyes.

widespread usage in different industries including textiles, food, glass, printing, cosmetics, plastics, rubber, etc. [6–15]. However, a challenge arises when it comes to removing these dyes from the water they are used in Refs. [16,17]. In recent years, dyes have constituted a significant portion of environmental pollutants, particularly in water [13,18–20]. Removal of complex organic dyes such as rhodamine B (RhB) and Methylene blue (MB) from water is a global issue because they have harmful effects on the environment, particularly on human and aquatic organism health [21–24]. Methylene blue (MB) and rhodamine B (RhB) (Scheme 1) belong to the category of cationic organic dyes. They are toxic and carcinogenic and find use in different industries including plastics, printing, food, textiles, glass, and more [25–28]. Hence, it is vital to remove these hazardous organic substances from industrial effluents. They can have adverse impacts on human health, including symptoms like vomiting, nausea, and increased heart rate, while also affecting other living creatures [9,18,21,29,30]. Organic dyes can be removed by Different methods such as adsorption, ultrafiltration, oxidation, co-precipitation, etc. [8,14,31,32]. Among these, adsorption using an adsorbent is an economical, straightforward, and high-performance method for dye removal [1,33–35]. Over the past few decades, the adsorption of RhB and MB dyes from industrial effluents by means of adsorbents has been extensively studied as an excellent technique [8,36,37].

Layered double hydroxides (LDHs), part of the anionic clay family and often referred to as hydrotalcite, exhibit remarkable structural properties [35,38–40]. These include a high abundance of hydroxyl groups (OH) on the surface and the flexibility to adjust interlayer anions [41,42]. Recently, LDHs have found numerous applications across diverse fields, including catalysis, adsorption, medicine, drug release, and more [12,43–46]. LDHs are characterized by a general formula $[M^{2+}_{1-x}M^{3+}_{x}\,(OH)_2]^{x\,+}\,[A^{n-}]_{x/n}.mH_2O$, where M^{+2} and M^{+3} represent divalent and trivalent metal cations, respectively. A^{n-} denotes exchangeable interlayer anions, and x signifies the molar ratio of $M^{+3}/(M^{+2}+M^{+3})$ [47–51]. In addition, their remarkable attributes, including high adsorption capacity, cost-effective fabrication, and the capability for hydrogen bonding and electrostatic interactions, have garnered increasing interest across various applications, particularly in the field of adsorption [52–55]. The interlayer anions and positively charged layers of LDHs make LDH-based adsorbents highly effective in adsorbing contaminants (such as MB and RhB) from aqueous solutions [56–59].

Ethylenediaminetetraacetic acid (EDTA) is a stable agent known for its robust metal chelation capabilities, availability, and affordability. It is frequently employed to enhance and modify the surface properties of various adsorbents [60–62].

Melamine (MA) is an affordable and easily accessible organic substance that possesses exceptional chelating properties, offering significant potential for adsorption with contaminants [63]. As a result, it has been widely employed as a modifier in numerous organic and inorganic adsorbents, including MOFs [64], graphene hydrogels [65], etc. [65–67].

Nanocomposites consist of a blend of two or more components, enhancing their physical and chemical properties, including
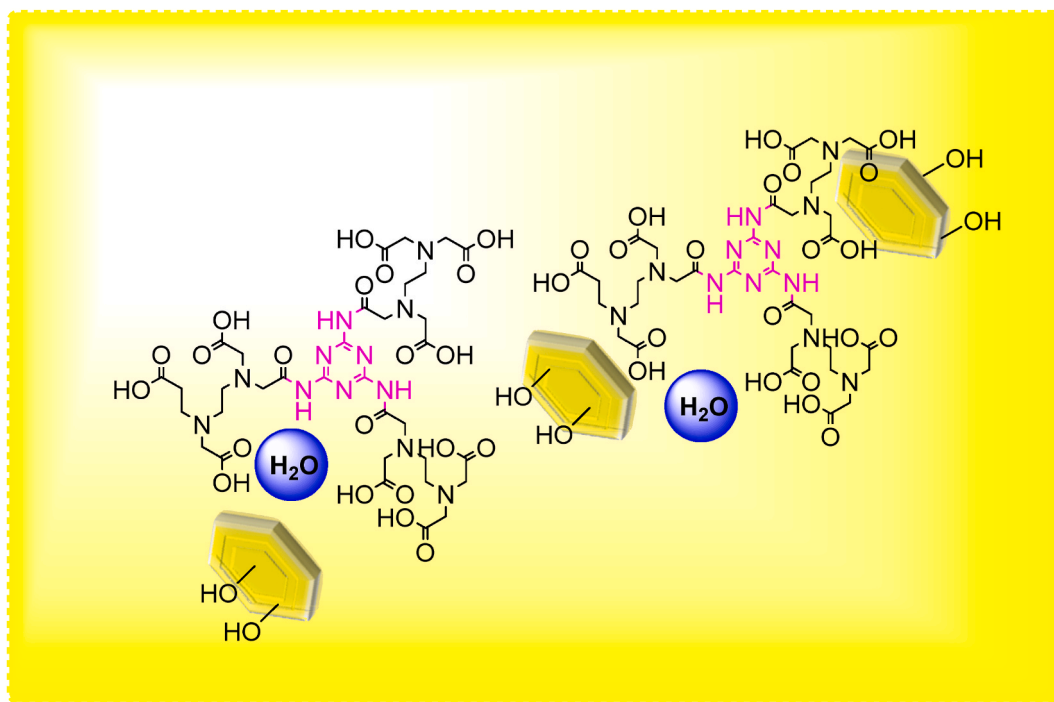
Scheme 2. The structure of the Mg–Al LDH@EDTA-MA nanocomposite.

mechanical characteristics, microscopic attributes, and high surface area to volume (S/V) ratio, relative to the individual components in isolation [68–70].

In this study, a novel, robust, and recyclable nanocomposite, Mg–Al LDH@EDTA-MA (Scheme 2), was successfully synthesized and characterized to be used for the efficient adsorption of RhB and MB dyes from water. EDTA-MA exhibits exceptional chelating capabilities, due to its abundance of NH and OH functional groups resulting in high adsorption efficiency. The Mg–Al LDH in the synthesized adsorbent enhances its environmentally friendly nature, achieved through a straightforward cost-effective preparation method. The facile preparation, easy and rapid dye adsorption, mild adsorption conditions, reusability, and high efficiency are unique properties of the prepared nanocomposite in comparison with previously reported adsorbents in the literature. To assess the synthesized adsorbent performance, the main affecting parameters including temperature, time, concentration, adsorbent dosage, and pH were optimized. Moreover, the study encompassed investigations into adsorption-desorption mechanisms, relevant isotherms, thermodynamic properties, and adsorption kinetics for a comprehensive analysis.

2. Experimental

2.1. Materials and methods

All the chemical materials were of high purity supplied by Aldrich or Merck and employed as-received. The Mg–Al LDH@EDTA-MA nanocomposite was characterized by FT-IR (Shimadzu 8400 s), X-ray diffractometer (TW 1800, $\lambda_{CuKa} = 1.54050$ Å), FE-SEM (TESCAN MIRA3), EDS (Numerix DXP-X10P), and TGA (STA504, Bahr Company).

2.2. Synthesis process of Mg–Al LDH

The synthesis of Mg–Al LDH was carried out through the utilization of urea-assisted co-precipitation technique [71,72]. Initially, a urea solution (100 mL, 3 M) was prepared and refluxed at 100 °C. Then, $Mg(NO_3)_2$ (5.131 g) and $Al(NO_3)_3$ (3.752 g) were added, followed by further refluxing for 12 h. Following this, the temperature was decreased to 94 °C, and the reaction was maintained for an additional 12 h without agitation. Afterward, the suspension of Mg–Al LDH underwent centrifugation and rinsing with deionized water until reaching a pH = 7. The resultant precipitate was subsequently subjected to drying at 80 °C in a conventional oven.

2.3. Preparation of EDTA-MA

EDTA (1 mmol, 0.291 g) was added to a flask containing acetonitrile (to dissolve the EDTA), followed by the addition of 1 mmol (0.155 g) 1-Ethyl-3-(3-dimethylaminopropyl)carbodiimide (EDCI) and stirring for 1 min at room temperature. Afterward,
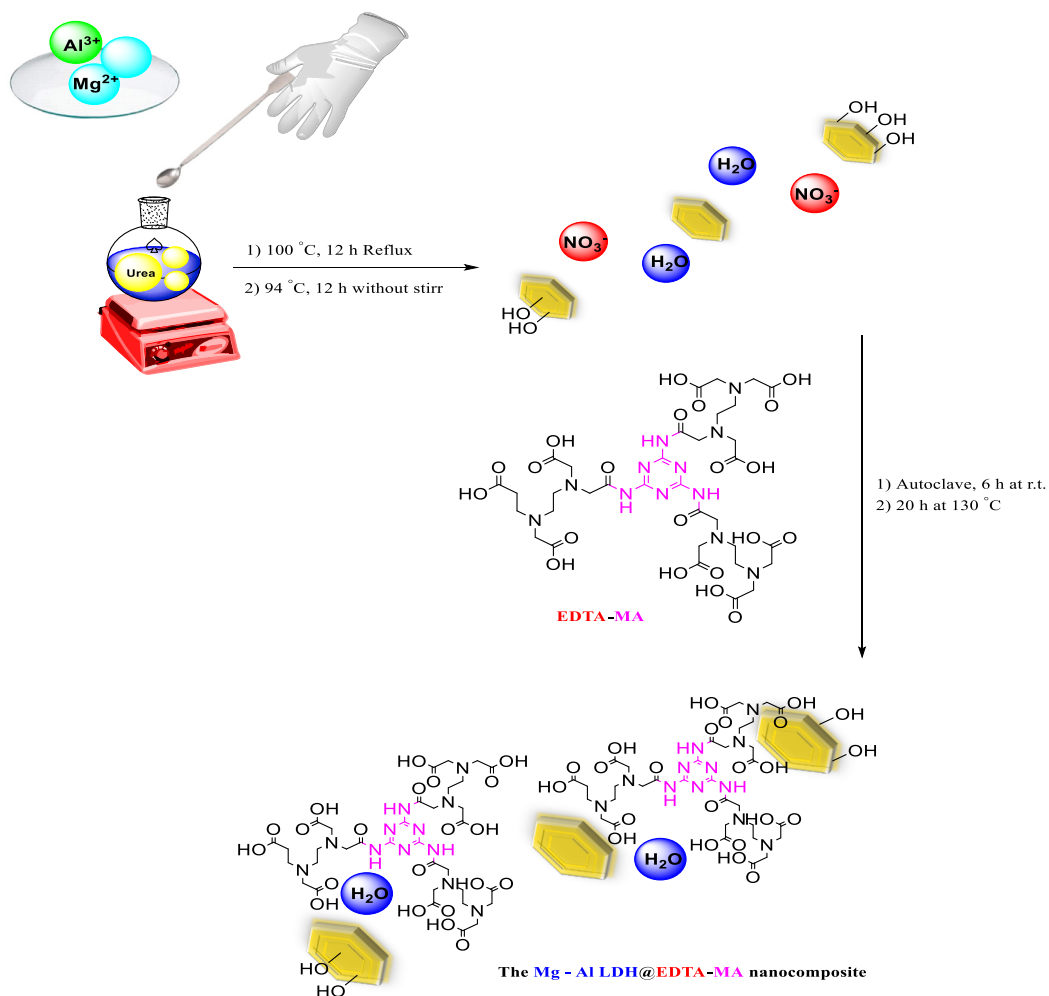
Scheme 3. Steps for the preparation of the Mg–Al LDH@EDTA-MA nanocomposite.

hydroxybenzotriazole (HOBT) (1 mmol, 0.135 g) was introduced and agitated for 1 h at ambient temperature. Following this, MA (0.396 mmol, 0.049 g) was incorporated and stirred for 24 h at room temperature. Subsequent to this, the solution was washed with CH$_3$CN and dried in an oven at 80 °C.

2.4. Synthesis process of the Mg–Al LDH@EDTA-MA nanocomposite

Mg–Al LDH (0.160 g) was dispersed in 10 mL water for 5 min in a flask. EDTA-MA (0.16 g) was also dispersed in 10 mL water for 5 min in another flask. Then, the solutions from the two flasks were combined in a beaker, 10 mL of water was added, and the mixture was stirred for 5 min at ambient temperature. A Teflon autoclave (50 mL) was used to prepare the Mg–Al LDH@EDTA-MA nano-composite. For this purpose, the mixed solution was kept at room temperature for 6 h, followed by heating at 130 $^\circ$C for 20 h. Finally, filtering, washing with DI water, and drying at 90 $^\circ$C was performed to obtain the desired product (Scheme 3).

2.5. Dye adsorption experiments

The main influencing parameters (i.e., concentration, time, adsorbent dosage, temperature, and pH) were examined to optimize the adsorption conditions. The amount of adsorption was calculated in the wavelengths of 664 nm and 554 nm for MB and RhB dyes, respectively. The coefficients of determination of the UV–Vis calibration curve are $R^2 = 0.9982$ and $R^2 = 0.9996$ for MB and RhB dyes, respectively. The adsorption capacity (mg/g) and adsorption percentage (removal percentage, R%) of MB and RhB dyes were calculated using Eqs. (1) and (2), respectively [2]:
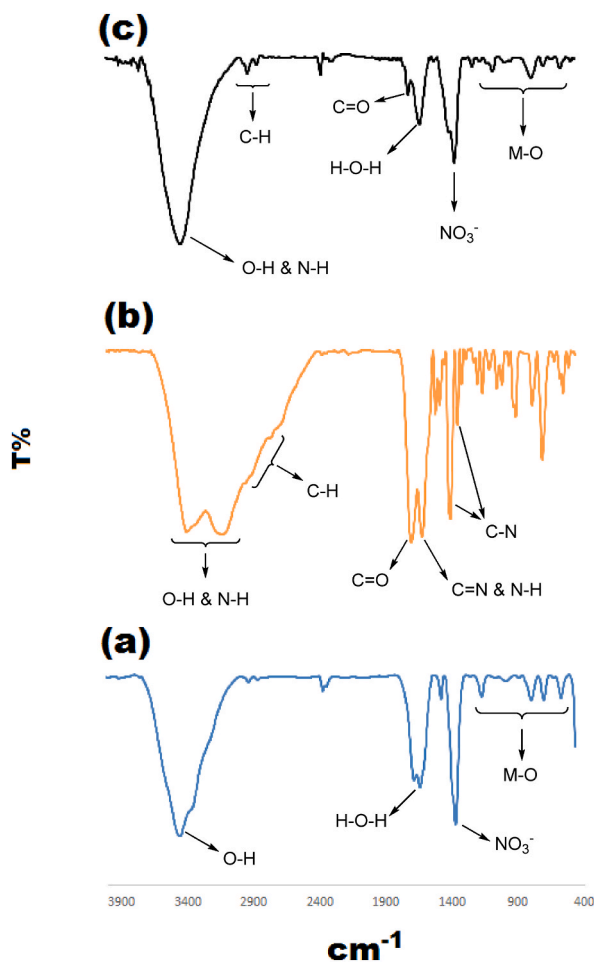
Fig. 1. The FT-IR spectra of Mg–Al LDH (**a**), EDTA-MA (**b**), and the Mg–Al LDH@EDTA-MA nanocomposite (**c**).

$$qe = \frac{(C_0 - C_e)V}{W} \tag{1}$$

$$R\% = \frac{(C_0 - C_e)}{C_0} \times 100 \tag{2}$$

where C_0 (mg/L) is the initial concentration and C_e (mg/L) is the equilibrium concentration of the MB and RhB dyes in the solution, W (mg) is the adsorbent mass, and V (mL) is the dye solution volume.

2.6. Dye desorption tests

Dye desorption tests were conducted to separate the adsorbent from the adsorbate dyes. This separation was achieved through a washing process using 0.1 moL/L HCl–NaCl mixture, followed by drying at 70 °C. The driving force behind the desorption process is ion exchange.

3. Results and discussion

3.1. Mg–Al LDH@EDTA-MA nanocomposite characterization

According to Fig. 1a, the FT-IR analysis of the Mg–Al layered double hydroxide reveals absorption bands at 3438 cm^{-1}, 1626 cm-1, and 1358 cm^{-1}, which correspond to the O–H stretching vibrations, bending vibrations of the interlayer H–O–H molecules, and asymmetric stretching modes of N–O in NO$_3^-$, respectively [73–76]. Moreover, the characteristic peaks ranging from 558 to 1162 cm^{-1} are associated with the stretching vibrations of metal-oxo group.

In the FT-IR spectrum of the EDTA-MA (Fig. 1b), the bands at 3394 cm^{-1} and 3112 cm^{-1} can be ascribed to stretching vibrations of
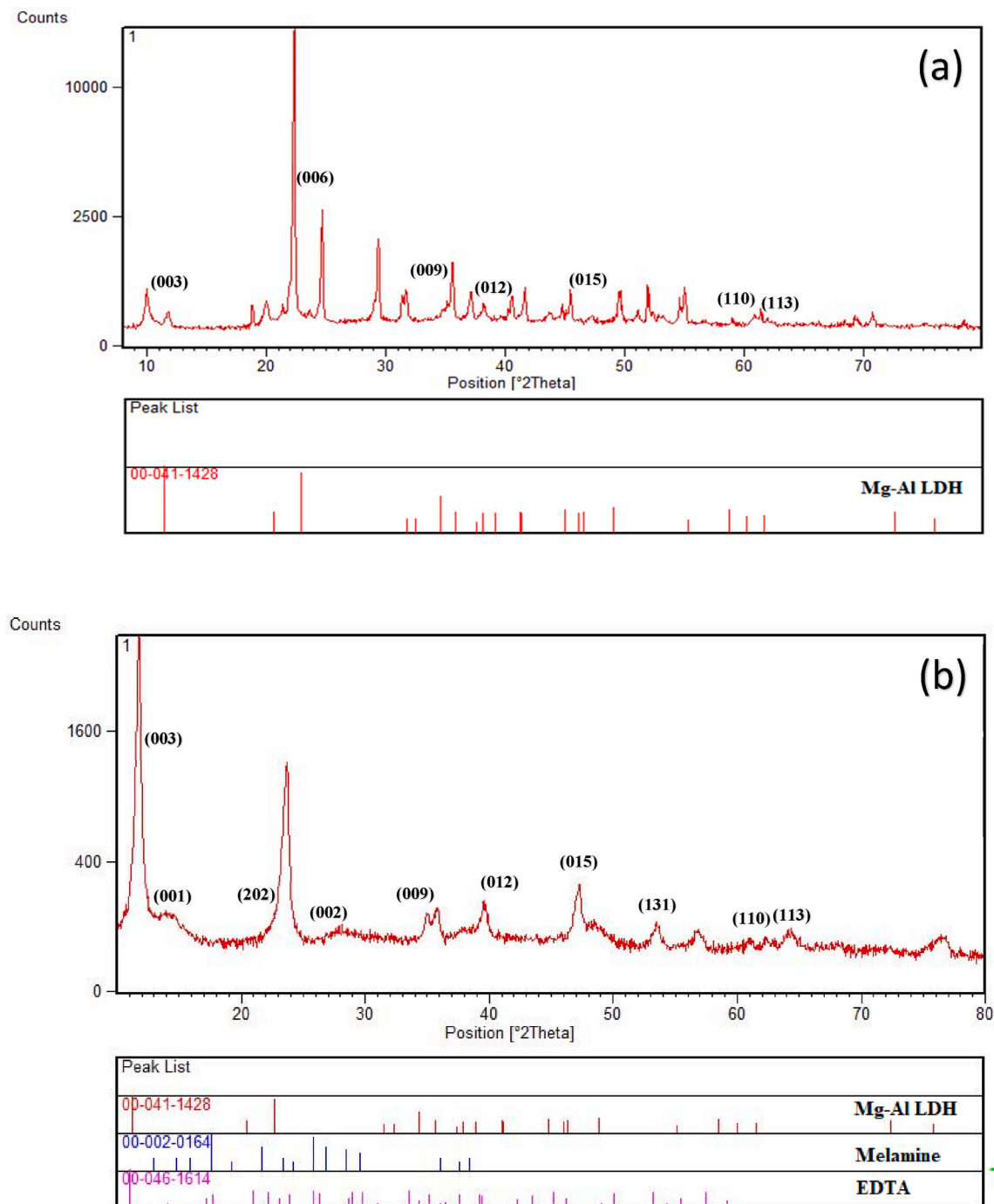
Fig. 2. The X-ray diffraction profiles of (**a**) Mg–Al LDH and (**b**) Mg–Al LDH@EDTA-MA.

N–H and O–H, respectively. Furthermore, the band at 2950 cm^{-1} belongs to the asymmetric stretching vibrations of C–H while that at 2916 cm^{-1} can be attributed to the symmetric stretching vibrations of C–H. The band at 1694 cm^{-1} is related to C=O stretching while that at 1608 cm^{-1} stems from C=N stretching and N–H bending vibrations. Additionally, the C–N aromatic stretching can be identified by the peaks at 1396 cm^{-1} and 1344 cm^{-1} [77].

FT-IR spectrum of the Mg–Al LDH@EDTA-MA nanocomposite is shown in Fig. 1c. The N–H and O–H stretching vibrations can be identified by the absorption band at 3430 cm^{-1}. Additionally, the absorption bands at 2924 cm^{-1} and 2856 cm^{-1} are attributed to the asymmetric and symmetric stretching vibrations of C–H bonds. Furthermore, the absorption band at 1712 cm^{-1} is related to the C=O stretching. The spectral peaks detected at 1624 cm^{-1}, 1360 cm^{-1}, and 1070-558 cm^{-1} have been assigned to the H$_2$O bending modes
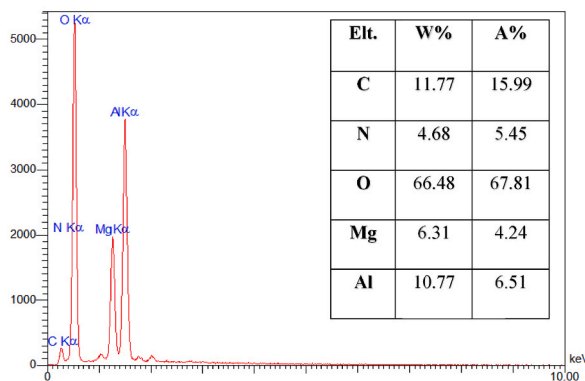
6

Fig. 3. EDS spectra for the synthesized Mg–Al LDH@EDTA-MA nanocomposite.

exhibited by the interlayer water molecules, the asymmetric stretching of N–O in NO_3^-, and the stretching vibrations of M − O, correspondingly. The presence of absorption bands at 3430 cm^{-1}, 2924-2856 cm^{-1}, and 1712 cm^{-1}, corresponding to N–H, C–H, and C═O stretching vibrations of EDTA-MA in the synthesized nanocomposite, provides evidence for the successful synthesis of the Mg–Al LDH@EDTA-MA nanocomposite. Furthermore, the shifts and changes in band intensity compared to the pure components indicate that Mg–Al LDH has successfully intercalated with EDTA-MA.

The XRD pattern illustrated in Fig. 2a depicts the crystallographic structure of Mg–Al LDH**.** The prominent diffraction peaks observed at 2θ values of 11.735° (003), 23.631° (006), 34.838° (009), 39.632° (012), 47.228° (015), 60.905° (110), and 61.39° (113) (JCPDS card No. 00-041-1428), respectively, confirm the crystal structure of the Mg–Al LDH [72,78]. As can be seen from XRD pattern of Mg–Al LDH@EDTA-MA nanocomposite in Fig. 2b, there are some peak shift and peak broadening in the XRD pattern which can be related to the intercalation process and possible interactions between the Mg–Al LDH layers. The four main diffraction peaks at 2θ of 11.735° (003), 34.838° (009), 60.905° (110), and 61.390° (113) (JCPDS card No. 00-041-1428) signifies the existence of the Mg–Al LDH within the framework [24,79]. The characteristic peaks at 2θ angles of 13.229° (001) and 27.112° (002), related to Melamine (JCPDS card No. 00-002-0164), and the peaks at 2θ angles of 10.942° (101), 22.316° (202) 53.361° (131), and 57.205° (113), attributed to EDTA (JCPDS card No. 00-046-1614), indicate the presence of EDTA-MA between the Mg–Al LDH layers, confirming the successful synthesis of the nanocomposite [80].

Fig. 3 shows the EDS spectra obtained for the synthesized Mg–Al LDH@EDTA-MA nanocomposite. The peaks related to all the elements of carbon (11.77 %), nitrogen (4.68 %), oxygen (66.48 %), magnesium (6.31 %), and aluminum (10.77 %) were detected in the synthesized nanocomposite. The peaks of magnesium (6.31 %) and aluminum (10.77 %) are specific to the Mg–Al LDH component of the nanocomposite. Furthermore, the peak of C (11.77 %) confirms the presence of EDTA-MA in the prepared nanocomposite.

Fig. 4 shows FE-SEM images obtained for Mg–Al LDH@EDTA-MA nanocomposite which display Mg–Al LDH hexagonal-like plates with a thickness of approximately 134 nm (Fig. 4b, c and f) [81,82]. A comparison between the images of the pristine Mg–Al LDH [81–84] and Mg–Al LDH@EDTA-MA nanocomposite reveals the successful incorporation of the EDTA-MA composite through an ion-exchange mechanism within the LDH layers (Fig. 4 b,c,f).

Fig. 5 displays the TGA curve of the Mg–Al LDH@EDTA-MA nanocomposite. Hydrogen bonding that presents between interlayer H_2O molecules and LDH results in an increase in the evaporation temperature of water. Consequently, the weight loss to 185 °C (~5 %) corresponds to the evaporation of the solvent. Considering that organic substances typically decompose at temperatures of about 400 °C, the strong hydrogen bonding between EDTA-MA and the OH groups in the Mg–Al LDH could be responsible for the exceptional heat resistance observed in the organic components of this nanocomposite. Accordingly, the weight losses occurring within the temperature ranges of 185–247 °C (~10 %) and 247–480 °C (~25 %) can be related to the thermal decomposition of entrapped EDTA-MA species [66]. The decomposition of LDH structure (dehydroxylation from Mg–Al LDH) results in the third weight loss observed at 480–800 °C [67,73]. In this range (480–800 °C), the curve slope is nearly constant which indicated that the LDH structure is stable at higher temperatures.

3.2. Adsorption studies

The amount of adsorbate that can be adsorbed on the adsorbent surface is known as the adsorption capacity. This parameter is profoundly influenced by various parameters, and understanding their effects is crucial for optimizing adsorption processes. These factors include initial concentration, adsorbent dosage, time, temperature, and solution pH.

3.2.1. Study of initial concentration

Concentration is a fundamental parameter in adsorption studies. Variations in concentration have a pronounced impact on adsorption kinetics and equilibrium, making it a logical starting point for optimization. For this purpose, 5 mg of adsorbent was dispersed in 100 mL solution containing 10–50 mg/L MB and RhB at 30 °C for 30 min at constant pH of 7. According to Fig. 6a, the adsorption capacity of the MB dye increases by increasing the dye concentration from 10 to 40 mg/L with a relatively steep slope.
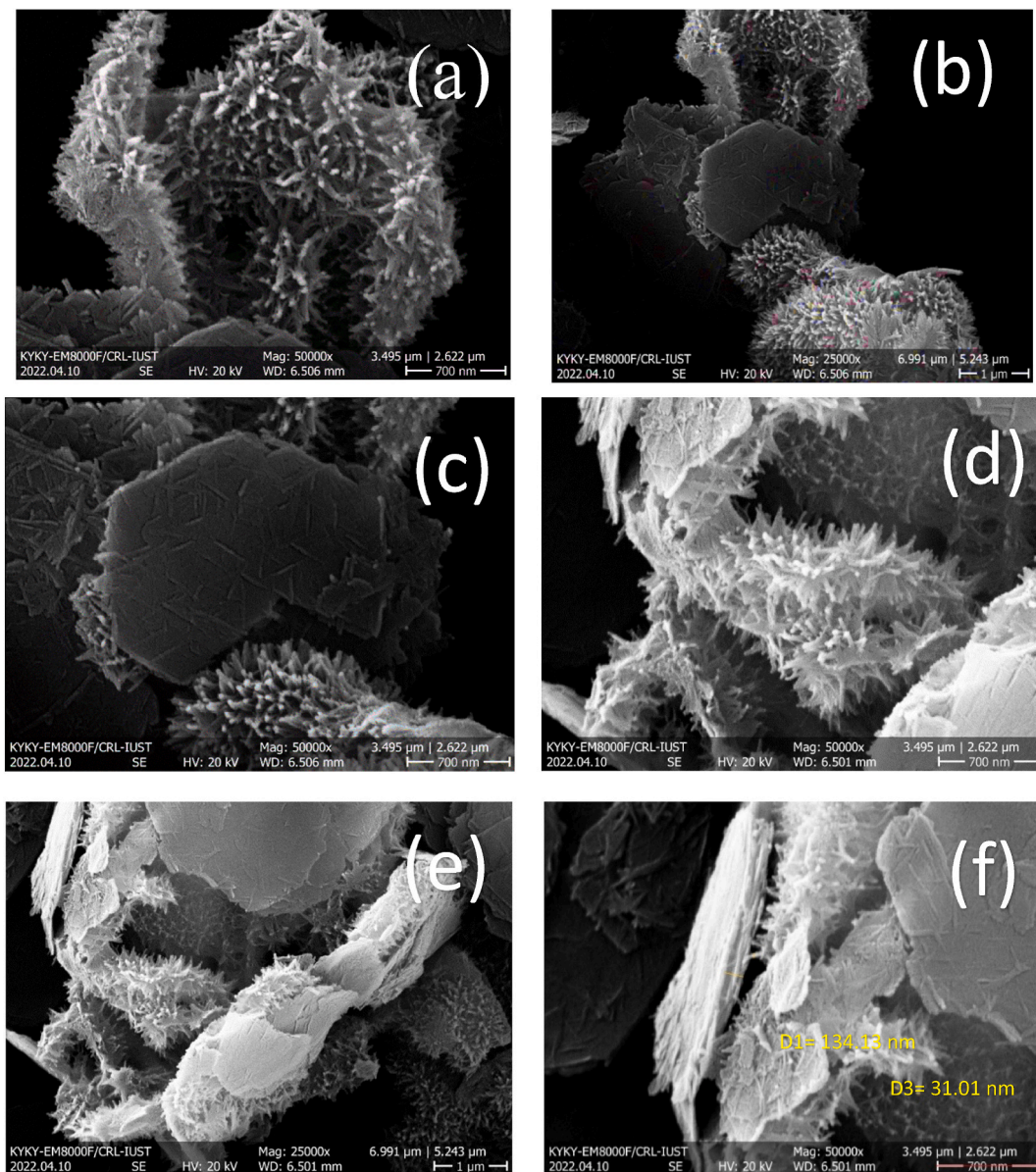
Fig. 4. FE-SEM images obtained from the Mg–Al LDH@EDTA-MA nanocomposite.
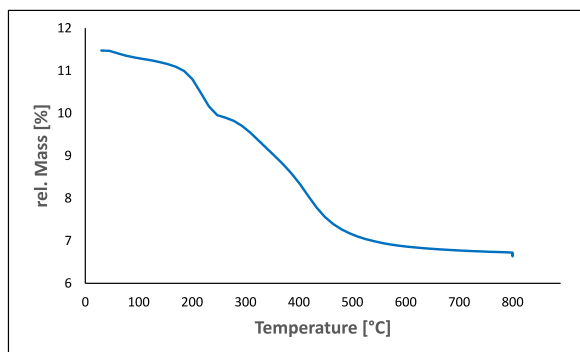
Fig. 5. The thermogravimetric analysis curve of the Mg–Al LDH@EDTA-MA nanocomposite.
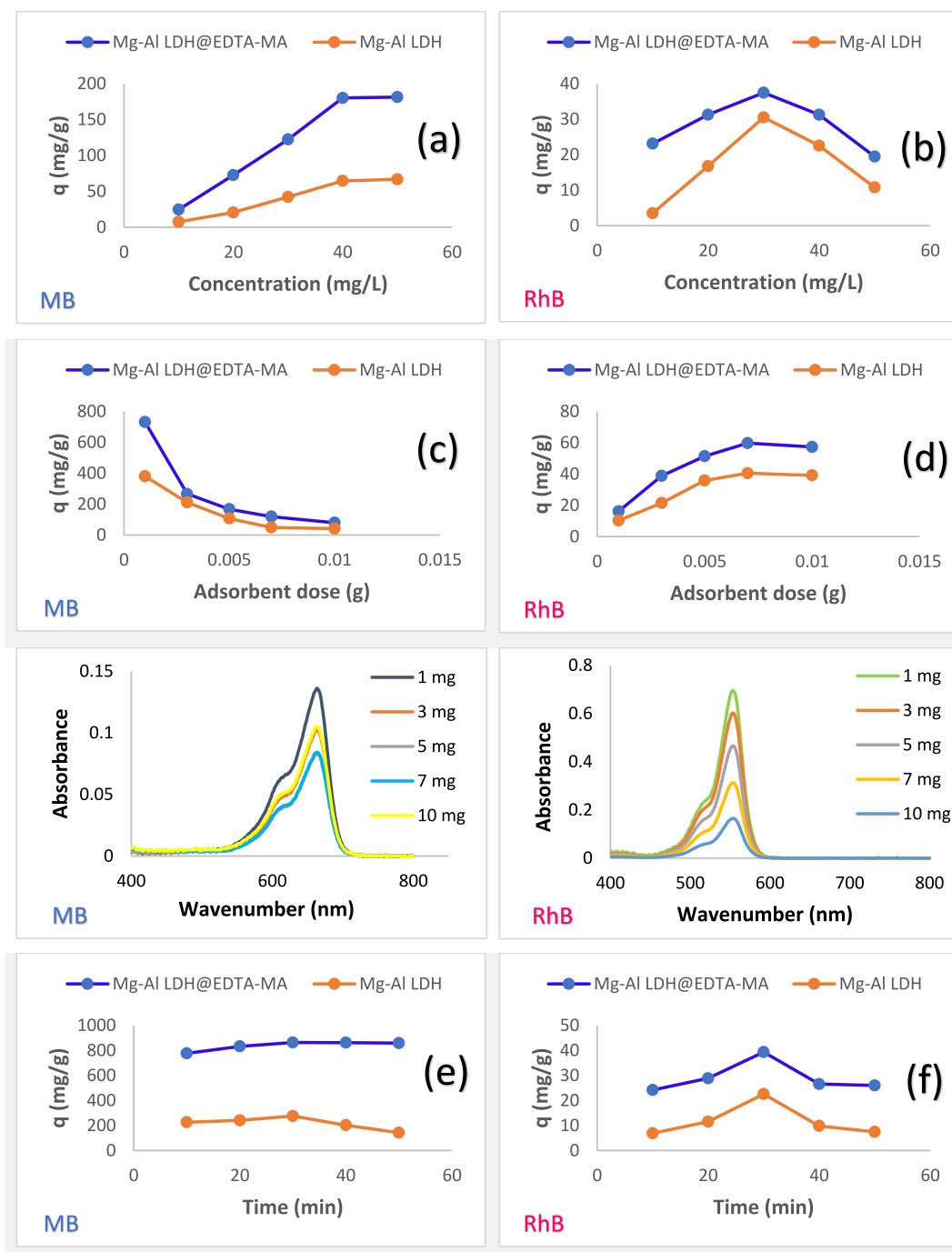
Fig. 6. The effect of different parameters on the adsorption of MB (**a, c, e, g, i**) and RhB (**b, d, f, h, j**) dyes; Concentration (**a, b**), adsorbent dosage (**c, d**), time (**e, f**), temperature (**g, h**), and pH (**i, j**). Conditions for MB adsorption ($C_0 = 10$ mg/L to 50 mg/L, pH = 7, T = 30 °C, adsorbent dosage = 5 mg, t = 30 min). Conditions for RhB adsorption: ($C_0 = 10$ mg/L to 50 mg/L, pH = 7, T = 30 °C, adsorbent dosage = 5 mg, t = 30 min).

However, the slope remains almost constant from 40 to 50 mg/L, which may be attributed to diffusion difficulties resulting from the accumulation of dye molecules. Additionally, the adsorption capacity of RhB is displayed in Fig. 6b in which the adsorption capacity first increases at the initial concentrations (10–30 mg/L), but decreases by further increasing the concentration from 30 to 50 mg/L. The maximal adsorptions for MB and RhB dyes were 40 mg/L and 30 mg/L, respectively. Therefore, the optimum Mg–Al LDH concentration for MB is 40 mg/L while that for RhB is 30 mg/L.
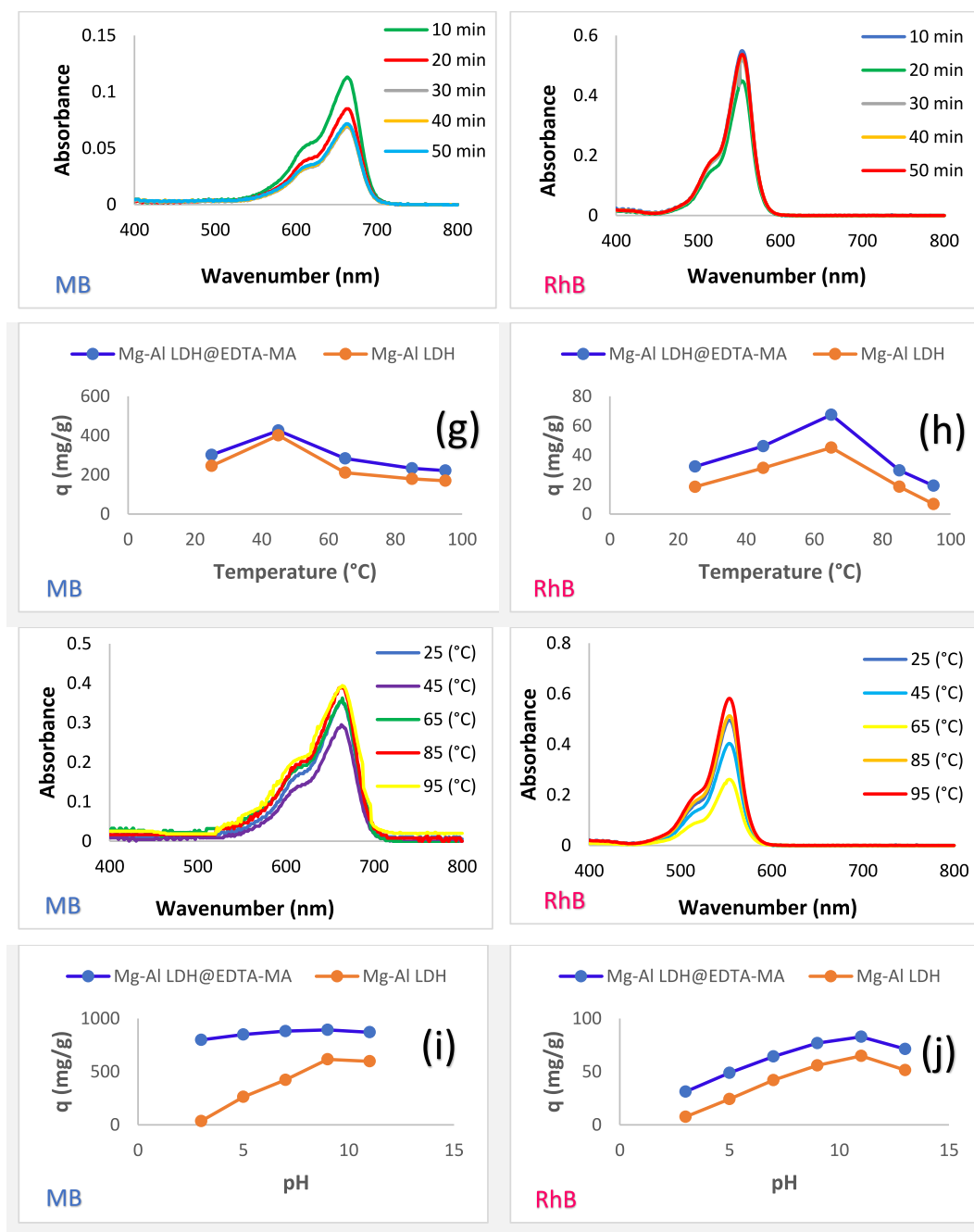
Fig. 6. (*continued*).

3.2.2. Study of adsorbent dosage

For investigating the influence of this parameter on the absorption capacity, different adsorbent doses (0.001 g–0.01 g) were used at constant concentration (C_0 = 40 mg/L), constant temperature (T = 30 °C), and pH = 7 for MB dye. These parameters for RhB dye were C_0 = 30 mg/L, T = 30 °C, and pH = 7. Fig. 6 (c, d) illustrates the effect of different adsorbent dosages on the adsorption capacity of both the Mg–Al LDH and the Mg–Al LDH@EDTA-MA. In the case of MB (Fig. 6c), the adsorption amount decreases with increasing adsorbent dosage, whereas for RhB (Fig. 6d), it increases up to 0.007 g. The maximum adsorption occurred at adsorbent dosages of 0.001 g and 0.007 g for MB and RhB dyes, respectively. The decrease in the adsorption can be related to the aggregation of the adsorbent particles and the limited availability of vacant space caused by the lower adsorbent surface area. Therefore, the optimum adsorption was achieved for 0.001 g Mg–Al LDH for MB and 0.007 g Mg–Al LDH for RhB.

Fig. 6. (*continued*).

3.2.3. Study of time

The adsorption of MB and RhB dyes using the Mg–Al LDH and the Mg–Al LDH@EDTA-MA was tested under conditions of $C_0 = 40$ mg/L, m = 0.001 g, T = 30 °C, and pH = 7 for MB, and $C_0 = 30$ mg/L, m = 0.007 g, T = 30 °C, and pH = 7 for RhB, at various times ranging from 10 min to 60 min. The adsorption capacities of the adsorbent for MB and RhB dyes as a fun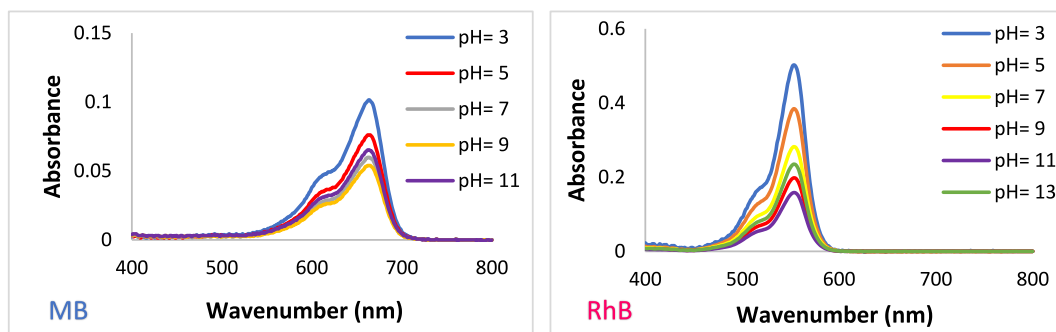ction of time are shown in Fig. 6 (**e**, **f**), and both exhibit an incremental increase from 10 to 30 min. For MB (Fig. 6e), a gradual decrease in adsorption was observed after 30 min, while for RhB (Fig. 6f), the decrease was more pronounced. The reduction in adsorption capacity could possibly be ascribed to the inadequate space available on the adsorbent. The maximum adsorption capacity was achieved at t = 30 min for both MB and RhB dyes. Therefore, the optimum contact time of the Mg–Al LDH was 30 min for MB and RhB dyes.

3.2.4. Study of temperature

The temperature is another key parameter in the adsorption process. Therefore, the adsorption capacity of the Mg–Al LDH and the Mg–Al LDH@EDTA-MA were studied at temperatures ranging from 25 °C to 95 °C under the conditions of $C_0 = 40$ mg/L, m = 0.001 g, t = 30 min, and pH = 7 for MB, and $C_0 = 30$ mg/L, m = 0.007 g, t = 30 min, and pH = 7 for RhB, as shown in Fig. 6 (**g**, **h**). The optimum adsorption temperature for MB (Fig. 6g) was observed at 45 °C. At higher temperatures, the adsorption capacity decreases until it reaches equilibrium. For RhB (Fig. 6h), the adsorption capacity increases by increasing the temperature from 25 °C to 65 °C, and the maximal adsorption capacity was obtained at 65 °C. Increasing the temperature enhances the diffusion of ions into the spaces between the Mg–Al LDH layers and causes the interactions between the adsorbent and the dye, thus increasing the adsorption capacity. Therefore, the optimum adsorption temperature of the Mg–Al LDH for MB and RhB dyes was 45 °C and 65 °C, respectively.

3.2.5. Study of solution pH

To achieve optimum pH values, the adsorption process using the Mg–Al LDH and Mg–Al LDH@EDTA-MA was tested at pH values of 3, 5, 7, 9, and 11 under the conditions of $C_0 = 40$ mg/L, m = 0.001 g, t = 30 min, and T = 45 °C for MB, and $C_0 = 30$ mg/L, m = 0.007 g, t = 30 min, and T = 65 °C for RhB (Fig. 6a–j). It can be seen that the adsorption capacity of MB and RhB dyes increases as the pH values increase, reaching an optimum point. The highest adsorption capacities for MB (Fig. 6i) and RhB (Fig. 6j) dyes were obtained at pH of 9 and 11, respectively. As a result, at alkaline pH levels, the electrostatic interactions between the negative charge on the Mg–Al LDH surface and the positive charge of MB and RhB dyes are increased, leading to higher adsorption capacity. The optimum pH values measured for Mg–Al LDH were 9 and 11, for MB and RhB dyes, respectively.

3.3. Adsorption isotherm models

In order to comprehend the interaction between the adsorbent and adsorbate, as well as the foundational significance of adsorption isotherms in the formulation of adsorbents, an investigation was conducted on Langmuir, Freundlich, and Temkin adsorption isotherms. The conditions applied for the adsorption of MB (pH = 9, T = 45 °C, t = 30 min, adsorbent dosage = 1 mg) and RhB (pH = 11, T = 60 °C, t = 30 min, adsorbent dosage = 7 mg) dye solutions on the Mg–Al LDH@EDTA-MA nanocomposite at various concentrations are illustrated in Fig. 7. Furthermore, parameters related to adsorption isotherms of the Mg–Al LDH and Mg–Al LDH@EDTA-MA were presented in Table 1. Given that the R^2 value of the Langmuir adsorption model for both dyes is higher than that of other adsorption isotherm models, it can be claimed that the adsorption of both dyes follows the Langmuir isotherm [73]. The maximum capacities for monolayer adsorption (q_{max}) on the Mg–Al LDH@EDTA-MA nanocomposite were 1111.103 mg/g for MB (at 45 °C) and 232.558 mg/g for RhB (at 60 °C). The comparison of the corresponding parameters in Table 1 shows that the chemical modification of Mg–Al LDH improves the adsorption capacity of the sample.

Eqs. (3) and (4) show the Langmuir and Freundlich adsorption isotherms, respectively. Additionally, Eq. (5) and (**6**) depict the Temkin adsorption isotherm:

$$\frac{C_e}{q_e} = \frac{1}{K_L q_m} + \frac{1}{q_m} C_e \quad \text{Langmuir} \tag{3}$$
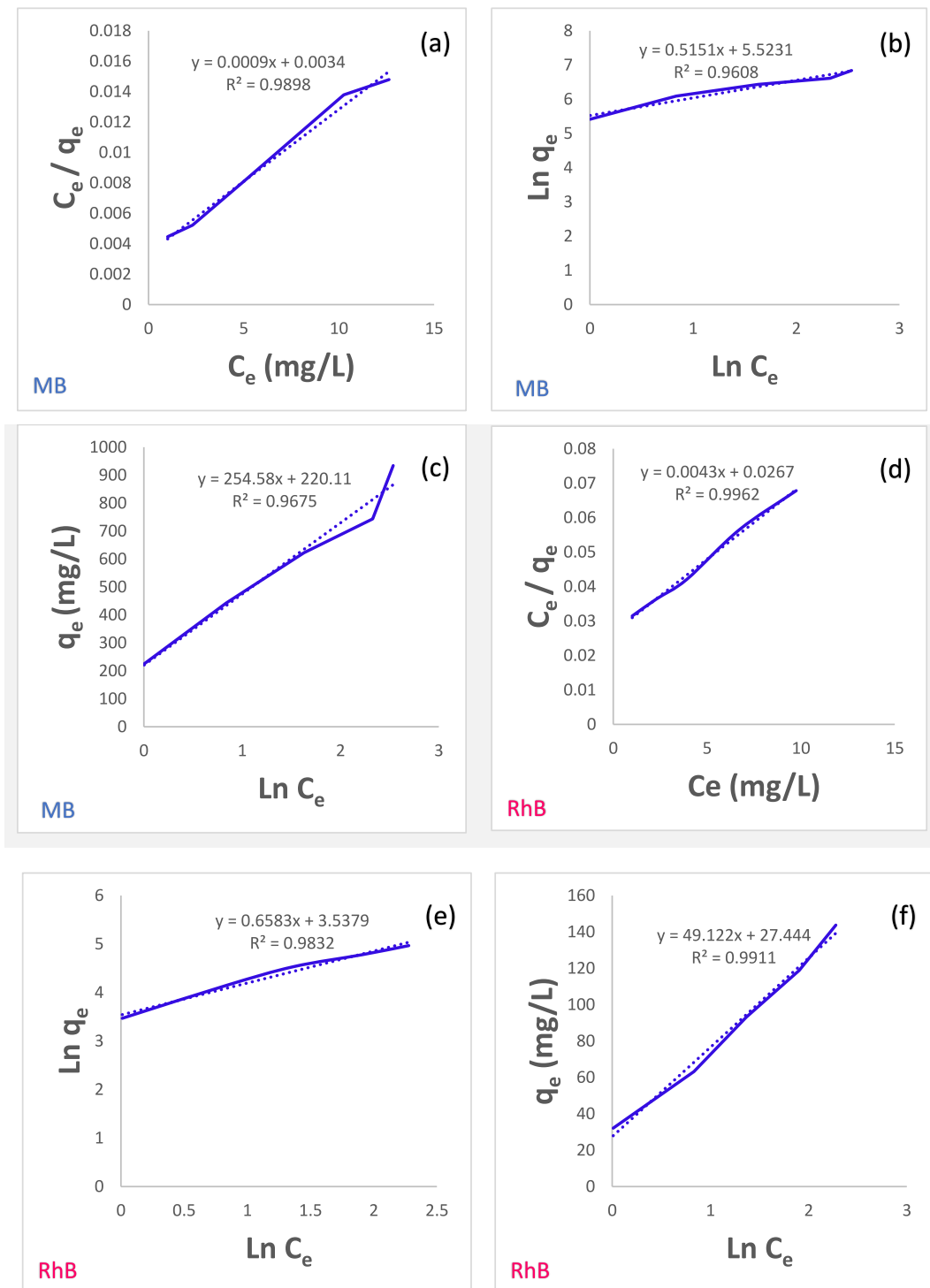
Fig. 7. Equilibrium studies of MB and RhB dyes adsorption; Langmuir (**a**), Freundlich (**b**), and Temkin (**c**), ($C_0 = 10$ mg/L to 50 mg/L, pH = 9, T = 45 °C, t = 30 min, adsorbent dosage = 1 mg) for MB and Langmuir (**d**), Freundlich (**e**) and Temkin (**f**) isotherm models, ($C_0 = 10$ mg/L to 50 mg/L, pH = 11, T = 60 °C, t = 30 min, adsorbent dosage = 7 mg) for RhB.

$$ln\ q_e = ln\ K_F + \left(\frac{1}{n}\right)ln\ C_e \quad \text{Freundlich} \qquad\qquad (4)$$

Table 1
Langmuir, Freundlich, and Temkin isotherm parameters for MB and RhB via Mg–Al LDH and the Mg–Al LDH@EDTA-MA.

Models	Parameters	Mg–Al LDH		Mg–Al LDH@EDTA-MA	
		MB	RhB	MB	RhB
Langmuir	q_{max}	711.25	45.137	1111.103	232.558
	K_L	0.271	0.165	0.265	0.160
	R^2	0.9735	0.9867	0.9898	0.9962
Freundlich	K_F	249.704	34.395	250.41	34.39
	n	1.98	1.56	1.94	1.52
	R^2	0.9592	0.9741	0.9608	0.9832
Temkin	K_T	2.29	1.71	2.37	1.75
	B	229.16	29.82	254.58	49.12
	R^2	0.9611	0.9821	0.9675	0.9911

Table 2
Kinetic parameters for the adsorption of MB ($C_0 = 40$ mg/L, pH = 9, T = 45 °C, adsorbent dosage = 1 mg, t = 10, 20, 30, 40, and 50 min) and RB ($C_0 = 30$ mg/L, pH = 11, T = 60 °C, adsorbent dosage = 7 mg, t = 10, 20, 30, 40, and 50 min) dyes on the Mg–Al LDH@EDTA-MA nanocomposite.

Dyes	Pseudo-first-order model			Pseudo-second-order model		
	k_1 (1/min)	q_e (mg/g)	R^2	k_2 (g/(mg.min))	q_e (mg/g)	R^2
MB	0.102	240.602	0.99	0.0007	909.091	1
RhB	0.037	21.948	0.99	0.040	26.042	1

$$q_e = BT \ln K_t + BT \ln C_e \quad \text{Temkin} \tag{5}$$

$$bT = \frac{(RT)}{(BT)} \quad \text{Temkin} \tag{6}$$

where q_m is the maximum adsorption capacity (mg/g), K_L is the Langmuir constant, q_e (mg/g) is the equilibrium concentration of the dyes on the adsorbent, and C_e (mg/L) is the equilibrium concentration of the dyes in the solution, K_F and n are Freundlich constants. In **Eqs. (5) and (6)**, bT and BT are constants, and K_t is the Temkin adsorption potential (L/g).

3.4. Study of adsorption kinetics

Kinetic data play a significant role in adsorption. Therefore, the pseudo-first-order as well as pseudo-second-order kinetic models were studied, as represented by **Eqs. (7) and (8)**, respectively.

$$\log(q_e - q_t) = \log q_e - \left(\frac{k_1 . t}{2.303}\right) \tag{7}$$

$$\frac{t}{q_t} = \frac{1}{k_2 q_e^2} + \left(\frac{1}{q_e}\right) t \tag{8}$$

where q_e is the adsorption capacity at equilibrium (mg/g), and q_t is the adsorption capacity at time t (min). Also, k_1 (min^{-1}) and k_2 (g/(mg. min)) stand as the rate coefficients for pseudo-first-order and pseudo-second-order adsorption, respectively.

This study was done with the adsorbent dosage of 0.001 g at pH = 9, T = 45 °C, and C_0 of 40 mg/L for MB. Additionally, the adsorbent dosage of 0.007 g at pH = 11, T = 60 °C, and C_0 of 30 mg/L were used for RhB. The mixtures were stirred at different times of 10, 20, 30, 40, and 50 min for both dyes, followed by the filtering of the samples to separate the adsorbent.

The kinetic parameter values for the adsorption of MB and RhB dyes onto the Mg–Al LDH@EDTA-MA nanocomposite were presented in Table 2. The correlation factor (R^2) of the pseudo-second-order kinetic model, exceeds that of the pseudo-first-order model. Consequently, it is inferred that the adsorption of both MB and RhB dyes on the nanocomposite conforms to a pseudo-second-order kinetic model [18,73,85].

3.5. Thermodynamic studies

To determine whether processes were spontaneous or non-spontaneous and whether they were exothermic or endothermic, thermodynamic parameters such as $\Delta G°$, $\Delta H°$, and $\Delta S°$ were examined using **Eqs. 9 and 10**. The results of this analysis are summarized in Table 3.

$$\ln K_d = \frac{\Delta S}{R} - \frac{\Delta H}{RT} \tag{9}$$

Table 3

Thermodynamic parameters for the adsorption of MB ($C_0 = 40$ mg/L, pH = 9, T = 25, 45, 65, 85, and 95 °C, adsorbent dosage = 1 mg, t = 30 min) and RhB ($C_0 = 30$ mg/L, pH = 11, T = 25, 45, 65, 85, and 95 °C, adsorbent dosage = 7 mg, t = 30 min) dyes on the Mg–Al LDH/EDTA-MA nanocomposite.

| Dyes	$\Delta G°$ (KJ/mol)					$\Delta H°$ (KJ/mol)	$\Delta S°$ (J/mol.K)
	298	318	338	358	368		
MB	−11.04	−10.95	−10.86	−10.76	−10.72	−12.42	−4.64
RhB	−6.52	−5.22	−3.92	−2.62	−1.98	−25.84	−64.84

Table 4

Comparison of the adsorption capacity of the Mg–Al LDH@EDTA-MA nanocomposite for the adsorption of MB and RhB dyes with other reported adsorbents in the literature.

Entry	Adsorbent	Adsorption capacity (mg/g)		Reference
		MB	RhB	
1	SCHMs[a]	88.3333	–	[86]
2	ACB[b]	136.99	–	[87]
3	Cellulose/MWCNTs/Fe3O4 composite beads	285.71	–	[88]
4	CMC/GOCOOH composite microbeads	183.23	–	[27]
5	PT-GO bio-adsorbent	444.44	–	[89]
6	SCBAC	–	5.3	[90]
7	γ-Fe2O3@Mt	–	209.20	[91]
8	ASC	–	123.46	[92]
9	acid modified banana pee	–	9.5220	[93]
10	**This work**	**1111.103**	**232.558**	**-**

[a] Magnetic starch-based composite hydrogel microsphe

[b] Activated carbon made from Moringa oleifera leaf.
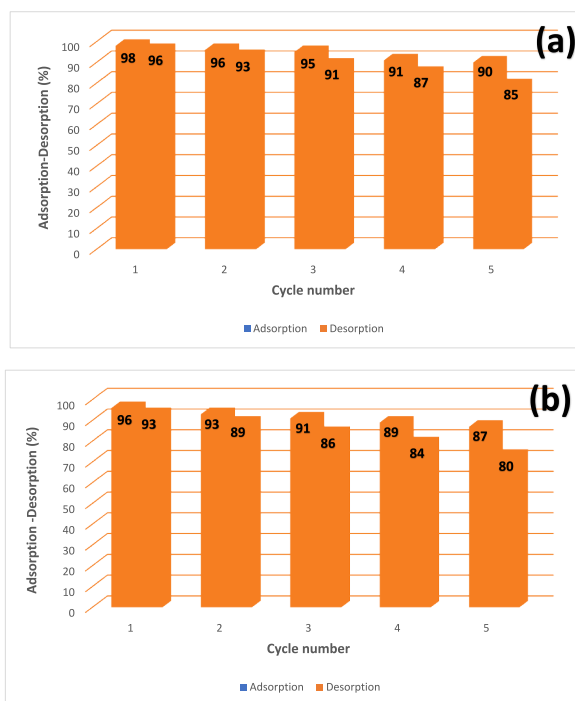
Fig. 8. The adsorption-desorption cycles for the removal of MB (a) and RhB (b) dyes on the Mg–Al LDH@EDTA-MA nanocomposite.

$$\Delta G° = \Delta H° - T\Delta S° \tag{10}$$

In the equation, T (K) denotes the temperature, while R signifies the gas constant. Based on the results obtained in Table 3, $\Delta G°$ is < 0 for both MB and RhB dyes, indicating the spontaneity of the process. Furthermore, $\Delta H°$ is < 0, confirming the exothermic nature of the process for both dyes.
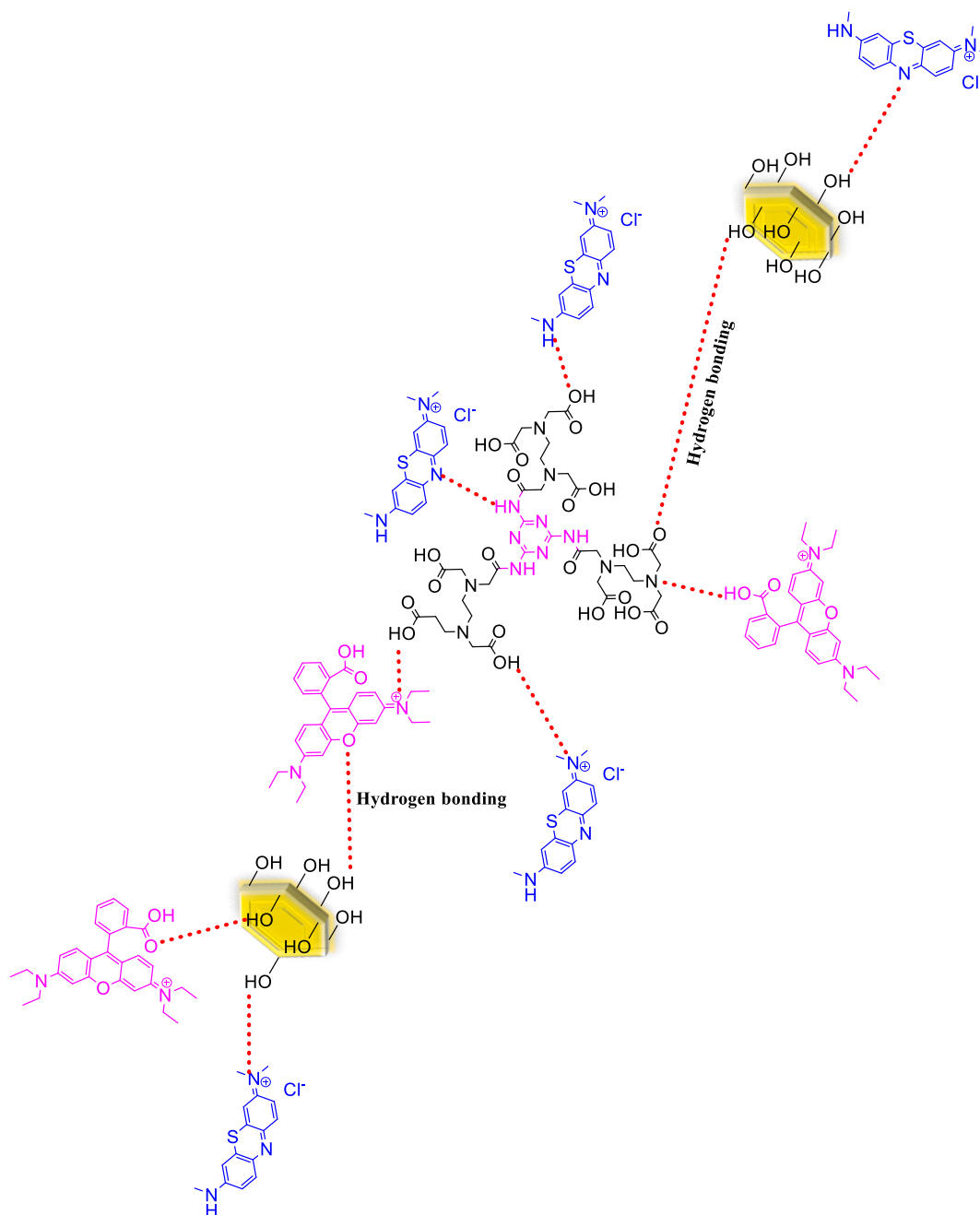
Scheme 4. The possible mechanism for the adsorption of MB and RhB dyes by the Mg–Al LDH@EDTA-MA nanocomposite.

3.6. Comparison of the maximum adsorption capacity with other reported adsorbents

Table 4 presents a comparison of the maximum adsorption capacity of the Mg–Al LDH@EDTA-MA nanocomposite for MB and RhB dyes adsorption with previously reported adsorbents in the literature. The facile preparation, easy and rapid dye adsorption, mild adsorption conditions, reusability, and high efficiency are unique properties of the prepared nanocomposite.

3.7. Recycling studies

Reusability is one of the most crucial parameters to investigate the applicability of the nanocomposite for the adsorption of MB and RhB dyes. To assess this, desorption tests were conducted to separate the adsorbent from the adsorbate dyes. This separation was achieved through a washing process using 0.1 moL/L HCl–NaCl mixture, followed by drying at 70 °C. The driving force behind the

desorption process is ion exchange [94,95]. Remarkably, even after four cycles of reactions, the Mg–Al LDH@EDTA-MA nanocomposite demonstrated high reusability, with an adsorption capacity of 90 % for MB and 87 % for RhB dyes, indicating a minimal loss in adsorption capacity (Fig. 8a and b). The adsorption capacity of the nanocomposite per adsorption-desorption cycle for the four cycles was 96 %, 95 %, 91 %, and 90 % for MB, and 93 %, 91 %, 89 %, and 87 % for RhB, respectively. In Fig. 8, the adsorption percentages indicate the amount of dye adsorption capacity for the adsorbent. Similarly, the desorption percentages reflect the amount of desorption of the adsorbate dyes from the adsorbent.

3.8. Adsorption mechanism

Scheme 4 illustrates the proposed adsorption mechanism of MB and RhB dyes. Based on the structure of Mg–Al LDH@EDTA-MA nanocomposite the adsorption mechanism involves both chemical and physical processes. EDTA is known for its chelating properties and its ability to form stable complexes. When intercalated into the Mg–Al LDH, EDTA-MA can provide active sites for chemical interactions with MB and RhB dyes, leading to the formation of coordination complexes between the dyes and the functional groups of EDTA. The layered structure of Mg–Al LDH provides a large surface area with abundant surface hydroxyl groups, which can facilitate the physical adsorption of dye molecules via hydrogen bonding and electrostatic interactions. The latter occurs as a result of the presence of negative charges on the LDH surface and positive charges of MB and RhB dyes in alkaline pH [73,84,96].

4. Conclusions

In summary, the Mg–Al LDH@EDTA-MA nanocomposite was successfully synthesized for removing MB and RhB from water. The unique properties of the prepared adsorbent include rapid and easy adsorption of MB and RhB dyes, facile preparation, mild adsorption conditions, high efficiency, and recyclability for up to 4 cycles without a significant drop-in activity. The maximum adsorption capacity for MB and RhB dyes is 1111.103 mg/g and 232.558 mg/g, respectively. Adsorption of both methylene blue and rhodamine B dyes followed pseudo-second-order adsorption kinetics, and their adsorption followed the Langmuir isotherm. Furthermore, thermodynamic analysis data revealed that the adsorption of MB and RhB dyes by Mg–Al LDH@EDTA-MA nanocomposite is spontaneous and exothermic.

Data availability

Data will be made available on request.

CRediT authorship contribution statement

Mohammad Ara: Writing – original draft, Visualization, Software, Methodology, Investigation, Formal analysis, Data curation. **Hossein Ghafuri:** Writing – review & editing, Validation, Supervision, Project administration.

Declaration of competing interest

The authors declare that they have no known competing financial interests or personal relationships that could have appeared to influence the work reported in this paper.

Appendix A. Supplementary data

Supplementary data to this article can be found online at https://doi.org/10.1016/j.heliyon.2024.e32447.

References

[1] C.R. Holkar, A.J. Jadhav, D.V. Pinjari, N.M. Mahamuni, A.B. Pandit, A critical review on textile wastewater treatments: possible approaches, J. Environ. Manage. 182 (2016) 351–366.
[2] A. Nasiri, N. Golestani, S. Rajabi, M. Hashemi, Facile and green synthesis of recyclable, environmentally friendly, chemically stable, and cost-effective magnetic nanohybrid adsorbent for tetracycline adsorption, Heliyon 10 (2024) e24179.
[3] M. Sajid, I. Ihsanullah, Magnetic layered double hydroxide-based composites as sustainable adsorbent materials for water treatment applications: progress, challenges, and outlook, Sci. Total Environ. 880 (2023) 163299.
[4] J. Singh, S. Juneja, R. Soni, J. Bhattacharya, Sunlight mediated enhanced photocatalytic activity of TiO2 nanoparticles functionalized CuO-Cu2O nanorods for removal of methylene blue and oxytetracycline hydrochloride, J. Colloid Interface Sci. 590 (2021) 60–71.
[5] M. Ghaedi, A. Ghaedi, F. Abdi, M. Roosta, A. Vafaei, A. Asghari, Principal component analysis-adaptive neuro-fuzzy inference system modeling and genetic algorithm optimization of adsorption of methylene blue by activated carbon derived from Pistacia khinjuk, Ecotoxicol. Environ. Saf. 96 (2013) 110–117.
[6] X.S. Wang, Y. Zhou, Y. Jiang, C. Sun, The removal of basic dyes from aqueous solutions using agricultural by-products, J. Hazard Mater. 157 (2008) 374–385.
[7] N. Mohammed, H. Lian, M.S. Islam, M. Strong, Z. Shi, R.M. Berry, H.-Y. Yu, K.C. Tam, Selective adsorption and separation of organic dyes using functionalized cellulose nanocrystals, Chem. Eng. J. 417 (2021) 129237.
[8] N. Cao, X. Zhao, M. Gao, Z. Li, X. Ding, C. Li, K. Liu, X. Du, W. Li, J. Feng, Superior selective adsorption of MgO with abundant oxygen vacancies to removal and recycle reactive dyes, Sep. Purif. Technol. 275 (2021) 119236.

[9] M.I. Din, R. Khalid, J. Najeeb, Z. Hussain, Fundamentals and photocatalysis of methylene blue dye using various nanocatalytic assemblies-a critical review, J. Clean. Prod. 298 (2021) 126567.

[10] T. Huang, M. Yan, K. He, Z. Huang, G. Zeng, A. Chen, M. Peng, H. Li, L. Yuan, G. Chen, Efficient removal of methylene blue from aqueous solutions using magnetic graphene oxide modified zeolite, J. Colloid Interface Sci. 543 (2019) 43–51.

[11] N.A. El Essawy, S.M. Ali, H.A. Farag, A.H. Konsowa, M. Elnouby, H.A. Hamad, Green synthesis of graphene from recycled PET bottle wastes for use in the adsorption of dyes in aqueous solution, Ecotoxicol. Environ. Saf. 145 (2017) 57–68.

[12] H. Hu, J. Liu, Z. Xu, L. Zhang, B. Cheng, W. Ho, Hierarchical porous Ni/Co-LDH hollow dodecahedron with excellent adsorption property for Congo red and Cr (VI) ions, Appl. Surf. Sci. 478 (2019) 981–990.

[13] I.M. Sharaf, J. Laifi, S. Alraddadi, M. Saad, M. Koubesy, N.N. Elewa, H. Almohiy, Y.M. Ismail, A. Soldatov, Unraveling the effect of Cu doping on the structural and morphological properties and photocatalytic activity of ZrO2, Heliyon 10 (2024) e23848.

[14] J. Kim, G.-H. Bak, D.-Y. Yoo, Y.-I. Lee, Y.-G. Lee, K. Chon, Functionalization of pine sawdust biochars with Mg/Al layered double hydroxides to enhance adsorption capacity of synthetic azo dyes: adsorption mechanisms and reusability, Heliyon 9 (2023) e14142.

[15] F.P. de Freitas, A.M.M.L. Carvalho, A.d.C.O. Carneiro, M.A. de Magalhães, M.F. Xisto, W.D. Canal, Adsorption of neutral red dye by chitosan and activated carbon composite films, Heliyon 7 (2021) e07629.

[16] A.S. Abdulhameed, N.N.M.F. Hum, S. Rangabhashiyam, A.H. Jawad, L.D. Wilson, Z.M. Yaseen, A.A. Al-Kahtani, Z.A. Alothman, Statistical modeling and mechanistic pathway for methylene blue dye removal by high surface area and mesoporous grass-based activated carbon using K2CO3 activator, J. Environ. Chem. Eng. 9 (2021) 105530.

[17] D. Kang, C. Hu, Q. Zhu, Morphology controlled synthesis of hierarchical structured Fe2O3 from natural ilmenite and its high performance for dyes adsorption, Appl. Surf. Sci. 459 (2018) 327–335.

[18] S. Eftekhari, A. Habibi-Yangjeh, S. Sohrabnezhad, Application of AlMCM-41 for competitive adsorption of methylene blue and rhodamine B: thermodynamic and kinetic studies, J. Hazard Mater. 178 (2010) 349–355.

[19] A.S. Eltaweil, Eman Abd El-Monaem, G.M. El-Subruiti, M.M. Abd El-Latif, A.M. Omer, Fabrication of UiO-66/MIL-101 (Fe) binary MOF/carboxylated-GO composite for adsorptive removal of methylene blue dye from aqueous solutions, RSC Adv. 10 (2020) 19008–19019.

[20] U. Jinendra, D. Bilehal, B. Nagabhushana, A.P. Kumar, Adsorptive removal of Rhodamine B dye from aqueous solution by using graphene–based nickel nanocomposite, Heliyon 7 (2021) 06851.

[21] H. Hanafy, Adsorption of methylene blue and bright blue dyes on bayleaf capertree pods powder: understanding the adsorption mechanism by a theoretical study, J. Mol. Liq. 332 (2021) 115680.

[22] T. Taher, A. Yoshida, A. Lesbani, I. Kurnia, G. Guan, A. Abudula, W. Ueda, Adsorptive removal and photocatalytic decomposition of cationic dyes on niobium oxide with deformed orthorhombic structure, J. Hazard Mater. 415 (2021) 125635.

[23] A. Reghioua, D. Barkat, A.H. Jawad, A.S. Abdulhameed, A.A. Al-Kahtani, Z.A. Alothman, Parametric optimization by Box–Behnken design for synthesis of magnetic chitosan-benzil/ZnO/Fe3O4 nanocomposite and textile dye removal, J. Environ. Chem. Eng. 9 (2021) 105166.

[24] T. Waheed, P. Min, S. ud Din, P. Ahmad, M.U. Khandaker, S. Haq, K. Al-Mugren, F.U. Rehman, B. Akram, S. Nazir, Montmorillonite modified Ni/Mg/Al ternary layered double hydroxide nanoflowers with enhanced adsorption features, Heliyon 9 (2023) e20967.

[25] A.A. Al-Gheethi, Q.M. Azhar, P.S. Kumar, A.A. Yusuf, A.K. Al-Buriahi, R.M.S.R. Mohamed, M.M. Al-Shaibani, Sustainable approaches for removing Rhodamine B dye using agricultural waste adsorbents: a review, Chemosphere 287 (2022) 132080.

[26] C. Lops, A. Ancona, K. Di Cesare, B. Dumontel, N. Garino, G. Canavese, S. Hérnandez, V. Cauda, Sonophotocatalytic degradation mechanisms of Rhodamine B dye via radicals generation by micro-and nano-particles of ZnO, Appl. Catal. B Environ. 243 (2019) 629–640.

[27] A.S. Eltaweil, G.S. Elgarhy, G.M. El-Subruiti, A.M. Omer, Carboxymethyl cellulose/carboxylated graphene oxide composite microbeads for efficient adsorption of cationic methylene blue dye, Int. J. Biol. Macromol. 154 (2020) 307–318.

[28] A.A. Aryee, C. Gao, R. Han, L. Qu, Functionalized magnetic biocomposite based on peanut husk for the efficient sequestration of basic dyes in single and binary systems: adsorption mechanism and antibacterial study, J. Environ. Chem. Eng. 10 (2022) 108205.

[29] A.K. Al-Buriahi, A.A. Al-Gheethi, P.S. Kumar, R.M.S.R. Mohamed, H. Yusof, A.F. Alshalif, N.A. Khalifa, Elimination of rhodamine B from textile wastewater using nanoparticle photocatalysts: a review for sustainable approaches, Chemosphere 287 (2022) 132162.

[30] D. Jiang, R. Deng, G. Li, G. Zheng, H. Guo, Constructing an ultra-adsorbent based on the porous organic molecules of noria for the highly efficient adsorption of cationic dyes, RSC Adv. 10 (2020) 6185–6191.

[31] C. Yao, W. Zhang, L. Xu, M. Cheng, Y. Su, J. Xue, J. Liu, S. Hou, A facile synthesis of porous MXene-based freestanding film and its spectacular electrosorption performance for organic dyes, Sep. Purif. Technol. 263 (2021) 118365.

[32] S. Chang, Q. Zhang, Y. Lu, S. Wu, W. Wang, High-efficiency and selective adsorption of organic pollutants by magnetic CoFe2O4/graphene oxide adsorbents: experimental and molecular dynamics simulation study, Sep. Purif. Technol. 238 (2020) 116400.

[33] M.T. Yagub, T.K. Sen, S. Afroze, H.M. Ang, Dye and its removal from aqueous solution by adsorption: a review, Adv. Colloid Interface Sci. 209 (2014) 172–184.

[34] H. Bensalah, S.A. Younssi, M. Ouammou, A. Gurlo, M.F. Bekheet, Azo dye adsorption on an industrial waste-transformed hydroxyapatite adsorbent: kinetics, isotherms, mechanism and regeneration studies, J. Environ. Chem. Eng. 8 (2020) 103807.

[35] H. Hu, S. Wageh, A.A. Al-Ghamdi, S. Yang, Z. Tian, B. Cheng, W. Ho, NiFe-LDH nanosheet/carbon fiber nanocomposite with enhanced anionic dye adsorption performance, Appl. Surf. Sci. 511 (2020) 145570.

[36] T. Li, L. Liu, Z. Zhang, Z. Han, Preparation of nanofibrous metal-organic framework filter for rapid adsorption and selective separation of cationic dye from aqueous solution, Sep. Purif. Technol. 237 (2020) 116360.

[37] M.J. Nine, S. Kabiri, A.K. Sumona, T.T. Tung, M.M. Moussa, D. Losic, Superhydrophobic/superoleophilic natural fibres for continuous oil-water separation and interfacial dye-adsorption, Sep. Purif. Technol. 233 (2020) 116062.

[38] O. Rahmanian, M. Dinari, M.K. Abdolmaleki, Carbon quantum dots/layered double hydroxide hybrid for fast and efficient decontamination of Cd (II): the adsorption kinetics and isotherms, Appl. Surf. Sci. 428 (2018) 272–279.

[39] S. Bahraminejad, A. Pardakhty, I. Sharifi, A. Keyhani, E. Salarkia, M. Ranjbar, Synthesis and physicochemical characterization of Zn–Al layered double hydroxides (LDHs) as a delivery system for amphotericin B: in vitro and in silico antileishmanial study, Heliyon 9 (2023) e15308.

[40] A.S. Darwish, S.S. Mahmoud, F.E. Bayaumy, Microwave-assisted hydrothermal fabrication of hierarchical-stacked mesoporous decavanadate-intercalated ZnAl nanolayered double hydroxide to exterminate different developmental stages of Trichinella spiralis and Schistosoma mansoni in-vitro, Heliyon 9 (2023) e18110.

[41] J. Mittal, Recent progress in the synthesis of Layered Double Hydroxides and their application for the adsorptive removal of dyes: a review, J. Environ. Manage. 295 (2021) 113017.

[42] D. Lv, Layered double hydroxides functionalized by carbonaceous materials: from preparation to energy and environmental applications, Environ. Sci. Pollut. Res. 29 (2022) 30865–30891.

[43] M. Xu, M. Wei, Layered double hydroxide-based catalysts: recent advances in preparation, structure, and applications, Adv. Funct. Mater. 28 (2018) 1802943.

[44] C. Li, M. Wei, D.G. Evans, X. Duan, Layered double hydroxide-based nanomaterials as highly efficient catalysts and adsorbents, Small 10 (2014) 4469–4486.

[45] G. Fan, F. Li, D.G. Evans, X. Duan, Catalytic applications of layered double hydroxides: recent advances and perspectives, Chem. Soc. Rev. 43 (2014) 7040–7066.

[46] M.B. Poudel, G.P. Awasthi, H.J. Kim, Novel insight into the adsorption of Cr (VI) and Pb (II) ions by MOF derived Co-Al layered double hydroxide@ hematite nanorods on 3D porous carbon nanofiber network, Chem. Eng. J. 417 (2021) 129312.

[47] K.-W. Jung, S.Y. Lee, J.-W. Choi, M.-J. Hwang, W.G. Shim, Synthesis of Mg–Al layered double hydroxides-functionalized hydrochar composite via an in situ one-pot hydrothermal method for arsenate and phosphate removal: structural characterization and adsorption performance, Chem. Eng. J. 420 (2021) 129775.

[48] Z. Wang, Y. Tan, X. Duan, Y. Xie, H. Jin, X. Liu, L. Ma, Q. Gu, H. Wei, Pretreatment of membrane dye wastewater by CoFe-LDH-activated peroxymonosulfate: performance, degradation pathway, and mechanism, Chemosphere 313 (2023) 137346.

[49] Q. Yin, P. Lyu, G. Wang, B. Wang, Y. Li, Z. Zhou, Y. Guo, L. Li, N. Deng, Phosphorus-modified biochar cross-linked Mg-Al layered double-hydroxide stabilizer reduced U and Pb uptake by Indian mustard (Brassica juncea L.) in uranium contaminated soil, Ecotoxicol. Environ. Saf. 234 (2022) 113363.

[50] D. Chaillot, S. Bennici, J. Brendlé, Layered double hydroxides and LDH-derived materials in chosen environmental applications: a review, Environ. Sci. Pollut. Res. 28 (2021) 24375–24405.

[51] R. Keyikoğlu, A. Khataee, Y. Orooji, Degradation of emerging pollutants on bifunctional ZnFeV LDH@ graphite felt cathode through prominent catalytic activity in heterogeneous electrocatalytic processes, J. Environ. Manage. 342 (2023) 118090.

[52] Q. Wang, D. O'Hare, Recent advances in the synthesis and application of layered double hydroxide (LDH) nanosheets, Chem. Rev. 112 (2012) 4124–4155.

[53] J. Feng, Y. He, Y. Liu, Y. Du, D. Li, Supported catalysts based on layered double hydroxides for catalytic oxidation and hydrogenation: general functionality and promising application prospects, Chem. Soc. Rev. 44 (2015) 5291–5319.

[54] E. Esmaili, B. Samiey, C.-H. Cheng, Coupled adsorption-catalytic reduction of permanganate on Co–Al-layered double hydroxide for dye removal, J. Clean. Prod. 351 (2022) 131521.

[55] M.A. Salem, A.M. Khan, Y.K. Manea, A.A. Wani, Nano chromium embedded in f-CNT supported CoBi-LDH nanocomposites for selective adsorption of Pb2+ and hazardous organic dyes, Chemosphere 289 (2022) 133073.

[56] H. Xu, S. Zhu, M. Xia, F. Wang, Rapid and efficient removal of diclofenac sodium from aqueous solution via ternary core-shell CS@ PANI@ LDH composite: experimental and adsorption mechanism study, J. Hazard Mater. 402 (2021) 123815.

[57] R. Ma, X. Yan, X. Mi, Y. Wu, J. Qian, Q. Zhang, G.-H. Chen, Enhanced catalytic degradation of aqueous doxycycline (DOX) in Mg-Fe-LDH@ biochar composite-activated peroxymonosulfate system: performances, degradation pathways, mechanisms and environmental implications, Chem. Eng. J. 425 (2021) 131457.

[58] R. Bi, D. Yin, B. Lei, F. Chen, R. Zhang, W. Li, Mercaptocarboxylic acid intercalated MgAl layered double hydroxide adsorbents for removal of heavy metal ions and recycling of spent adsorbents for photocatalytic degradation of organic dyes, Sep. Purif. Technol. 289 (2022) 120741.

[59] J. Kang, F. Cintron-Colon, H. Kim, J. Kim, T. Varga, Y. Du, O. Qafoku, W. Um, T.G. Levitskaia, Removal of iodine (I− and IO3−) from aqueous solutions using CoAl and NiAl layered double hydroxides, Chem. Eng. J. 430 (2022) 132788.

[60] E. Repo, J.K. Warchoł, A. Bhatnagar, A. Mudhoo, M. Sillanpää, Aminopolycarboxylic acid functionalized adsorbents for heavy metals removal from water, Water Res. 47 (2013) 4812–4832.

[61] M.L.F.A. De Castro, M.S.B. Abad, D.A.G. Sumalinog, R.R.M. Abarca, P. Paoprasert, M.D.G. de Luna, Adsorption of methylene blue dye and Cu (II) ions on EDTA-modified bentonite: isotherm, kinetic and thermodynamic studies, Sustain. Environ. Res. 28 (2018) 197–205.

[62] A. Adibzadeh, M.R. Khodabakhshi, A. Maleki, Preparation of novel and recyclable chitosan-alumina nanocomposite as superabsorbent to remove diazinon and tetracycline contaminants from aqueous solution, Heliyon 10 (2024) e23139.

[63] N. Ghanbari, H. Ghafuri, Pyromellitic acid grafted to cross-linked LDH by dendritic units: an efficient and recyclable heterogeneous catalyst for green synthesis of 2, 3-dihydro quinazoline and dihydropyrimidinones derivatives, Heliyon 9 (2023) e20978.

[64] N. Yin, K. Wang, Z. Li, Novel melamine modified metal-organic frameworks for remarkably high removal of heavy metal Pb (II), Desalination 430 (2018) 120–127.

[65] X. Wang, R. Li, J. Liu, R. Chen, H. Zhang, Q. Liu, Z. Li, J. Wang, Melamine modified graphene hydrogels for the removal of uranium (VI) from aqueous solution, New J. Chem. 41 (2017) 10899–10907.

[66] Z.-C. Wu, Z.-Z. Wang, J. Liu, J.-H. Yin, S.-P. Kuang, A new porous magnetic chitosan modified by melamine for fast and efficient adsorption of Cu (II) ions, Int. J. Biol. Macromol. 81 (2015) 838–846.

[67] I.M. Kenawy, M.M. Eldefrawy, R.M. Eltabey, E. Zaki, Melamine grafted chitosan-montmorillonite nanocomposite for ferric ions adsorption: central composite design optimization study, J. Clean. Prod. 241 (2019) 118189.

[68] I.A. Kinloch, J. Suhr, J. Lou, R.J. Young, P.M. Ajayan, Composites with carbon nanotubes and graphene: an outlook, Science 362 (2018) 547–553.

[69] T. Hassan, A. Salam, A. Khan, S.U. Khan, H. Khanzada, M. Wasim, M.Q. Khan, I.S. Kim, Functional nanocomposites and their potential applications: a review, J. Polym. Res. 28 (2021) 1–22.

[70] Y. Zhang, Q. Chen, Z. Dai, Y. Dai, F. Xia, X. Zhang, Nanocomposite adhesive hydrogels: from design to application, J. Mater. Chem. B 9 (2021) 585–593.

[71] M.J. Mochane, S.I. Magagula, J.S. Sefadi, E.R. Sadiku, T.C. Mokhena, Morphology, thermal stability, and flammability properties of polymer-layered double hydroxide (LDH) nanocomposites: a Review, Crystals 10 (2020) 612.

[72] M. Ara, H. Ghafuri, N. Ghanbari, Copper (II) anchored on layered double hydroxide functionalized guanidine as a heterogeneous catalyst for the synthesis of tetrazole derivatives, Colloids Interface Sci. Commun. 53 (2023) 100704.

[73] N. Ghanbari, H. Ghafuri, Design and preparation the novel polymeric layered double hydroxide nanocomposite (LDH/Polymer) as an efficient and recyclable adsorbent for the removal of methylene blue dye from water, Environ. Technol. Innov. 26 (2022) 102377.

[74] J.T. Kloprogge, L. Hickey, R.L. Frost, FT-Raman and FT-IR spectroscopic study of synthetic Mg/Zn/Al-hydrotalcites, J. Raman Spectrosc. 35 (2004) 967–974.

[75] S. Kundu, M.K. Naskar, Al–Mg–Ca-layered double oxides for efficient removal of as (v) from water: the role of amides, J. Chem. Eng. Data 64 (2019) 1594–1604.

[76] S. Zhou, W. Li, J. Li, R. Li, Impact of inhibitor loaded with pigments content on properties of inorganic zinc rich coatings, Heliyon 10 (2024) e24739.

[77] A.M. Bakry, F.S. Awad, J.A. Bobb, A.A. Ibrahim, M.S. El-Shall, Melamine-based functionalized graphene oxide and zirconium phosphate for high performance removal of mercury and lead ions from water, RSC Adv. 10 (2020) 37883–37897.

[78] X. Wang, X. Zhu, X. Meng, Preparation of a Mg/Al/Fe layered supramolecular compound and application for removal of Cr (VI) from laboratory wastewater, RSC Adv. 7 (2017) 34984–34993.

[79] E. Abdollahi, A. Heidari, T. Mohammadi, A.A. Asadi, M.A. Tofighy, Application of Mg-Al LDH nanoparticles to enhance flux, hydrophilicity and antifouling properties of PVDF ultrafiltration membrane: experimental and modeling studies, Sep. Purif. Technol. 257 (2021) 117931.

[80] L. Chen, Q. Tu, X. Yang, X. Hu, X. Sun, H. Li, MgAl layered double hydroxides intercalated with edta: Cu (II) recovery and mechanism, ChemistrySelect 5 (2020) 11299–11304.

[81] G. Zheng, C. Wu, J. Wang, S. Mo, Y. Wang, Z. Zou, B. Zhou, F. Long, Facile synthesis of few-layer MoS 2 in MgAl-LDH layers for enhanced visible-light photocatalytic activity, RSC Adv. 9 (2019) 24280–24290.

[82] R. Pourfaraj, S.J. Fatemi, S.Y. Kazemi, P. Biparva, Synthesis of hexagonal mesoporous MgAl LDH nanoplatelets adsorbent for the effective adsorption of Brilliant Yellow, J. Colloid Interface Sci. 508 (2017) 65–74.

[83] H.N. Tran, C.-C. Lin, H.-P. Chao, Amino acids-intercalated Mg/Al layered double hydroxides as dual-electronic adsorbent for effective removal of cationic and oxyanionic metal ions, Sep. Purif. Technol. 192 (2018) 36–45.

[84] A.M. Aldawsari, I. Alsohaimi, H.M. Hassan, Z.E. Abdalla, I. Hassan, M.R. Berber, Tailoring an efficient nanocomposite of activated carbon-layered double hydroxide for elimination of water-soluble dyes, J. Alloys Compd. 857 (2021) 157551.

[85] J.E.T. Tech, Mg-Cr layered double hydroxide with intercalated oxalic anion for removal cationic dyes rhodamine B and methylene blue, J. Environ. Treat. Tech. 9 (2021) 85–94.

[86] W. Li, H. Wei, Y. Liu, S. Li, G. Wang, H. Han, Fabrication of novel starch-based composite hydrogel microspheres combining Diels-Alder reaction with spray drying for MB adsorption, J. Environ. Chem. Eng. 9 (2021) 105929.

[87] T.H. Do, N.Q. Dung, M.N. Chu, D. Van Kiet, T.T.K. Ngan, L. Van Tan, Study on methylene blue adsorption of activated carbon made from Moringa oleifera leaf, Mater. Today: Proc. 38 (2021) 3405–3413.

[88] F. Ding, P. Ren, G. Wang, S. Wu, Y. Du, X. Zou, Hollow cellulose-carbon nanotubes composite beads with aligned porous structure for fast methylene blue adsorption, Int. J. Biol. Macromol. 182 (2021) 750–759.

[89] Z. Wang, M. Gao, X. Li, J. Ning, Z. Zhou, G. Li, Efficient adsorption of methylene blue from aqueous solution by graphene oxide modified persimmon tannins, Mater. Sci. Eng. C 108 (2020) 110196.

[90] S.A. Mousavi, B. Kamarehie, A. Almasi, M. Darvishmotevalli, M. Salari, M. Moradnia, F. Azimi, M. Ghaderpoori, Z. Neyazi, M.A. Karami, Removal of Rhodamine B from aqueous solution by stalk corn activated carbon: adsorption and kinetic study, Biomass Convers. Biorefin. 13 (2023) 7927–7936.

[91] H. Ouachtak, R. El Haouti, A. El Guerdaoui, R. Haounati, E. Amaterz, A.A. Addi, F. Akbal, M.L. Taha, Experimental and molecular dynamics simulation study on the adsorption of Rhodamine B dye on magnetic montmorillonite composite γ-Fe2O3@ Mt, J. Mol. Liq. 309 (2020) 113142.

[92] W. Xiao, Z.N. Garba, S. Sun, I. Lawan, L. Wang, M. Lin, Z. Yuan, Preparation and evaluation of an effective activated carbon from white sugar for the adsorption of rhodamine B dye, J. Clean. Prod. 253 (2020) 119989.

[93] A.A. Oyekanmi, A. Ahmad, K. Hossain, M. Rafatullah, Adsorption of Rhodamine B dye from aqueous solution onto acid treated banana peel: response surface methodology, kinetics and isotherm studies, PLoS One 14 (2019) e0216878.

[94] M. Greluk, Z. Hubicki, Efficient removal of Acid Orange 7 dye from water using the strongly basic anion exchange resin Amberlite IRA-958, Desalination 278 (2011) 219–226.

[95] N.R. Palapa, R. Mohadi, A. Rachmat, Adsorption study of malachite green removal from aqueous solution using Cu/M3+ (M3+= Al, Cr) layered double hydroxide, Mediterr. J. Chem. 10 (2020) 33–45.

[96] T.J.M. Fraga, M.G. Ghislandi, M.N. Carvalho, M.A. da Motta Sobrinho, One step forward: how can functionalization enhance the adsorptive properties of graphene towards metallic ions and dyes? Environ. Res. 184 (2020) 109362.